Journal of Structural Geology 32 (2010) 792–802

Contents lists available at ScienceDirect

Journal of Structural Geology

journal homepage: www.elsevier.com/locate/jsg

Sequential deformation from serpentinite mylonite to metasomatic rocks along the Sashu Fault, SW Japan

Yusuke Soda*, Hideo Takagi

Department of Earth Sciences, Faculty of Education and Integrated Arts and Sciences, Waseda University, 1-6-1, Nishiwaseda, Shinjuku-ku, Tokyo 169-8050, Japan

ARTICLE INFO

Article history:
Received 17 October 2009
Received in revised form
28 April 2010
Accepted 12 May 2010
Available online 20 May 2010

Keywords:
Serpentinite mylonite
Serpentinite breccia
Metasomatic rocks
LPO of antigorite

ABSTRACT

The deformation of serpentinites along the Sashu Fault, Saganoseki Peninsula, SW Japan, involved both mylonitization and brecciation. The brecciation was accompanied by metasomatism, and the metasomatized rocks record additional ductile deformation. Serpentinite mylonite is composed mainly of antigorite, with minor magnetite and Cr-spinel. Foliation and lineation in this rock type are defined by the shape preferred orientation of antigorite and the alignment of fine-grained magnetite and carbonate minerals. The antigorite also shows a lattice preferred orientation (LPO), as measured with a universal stage, with *c* axes oriented near-perpendicular to the foliation and *b* axes oriented parallel to the lineation. Brecciation is concentrated in the reaction zone along the boundary between serpentinites and surrounding country rocks. Talc and chlorite schists developed in this zone as a result of associated metasomatism and deformation; consequently, they contain composite planar fabrics and drag folds. The breccias themselves are composed of serpentinite fragments cut by veins of calcite and talc. Analyses of fluid inclusions in calcite from the breccia indicate that brecciation occurred at 200–300 °C at depths of 3.8–11.8 km. Metasomatic reactions, particularly the formation of talc, contributed to weakening of this serpentinite-bearing fault zone.

1. Introduction

Serpentinite and its metasomatic products are important rocks to clarify the rheological properties along subduction zones (e.g. Peacock and Hyndman, 1999; Hermann et al., 2000) and along major faults such as the San Andreas Fault Zone (e.g. Andreani et al., 2005; Wibberley, 2007). It is possible that aseismic slip is facilitated by the occurrence of serpentinite along such shear zones, as indicated by the results of experimental studies (e.g. Moore et al., 1997; Reinen, 2000).

The serpentine mineral group consists of antigorite, lizardite, and chrysotile. Antigorite is stable below 600–700 °C, whereas lizardite and chrysotile are stable below 300 °C (O'Hanley, 1996; Ulmer and Trommsdorff, 1999). It has been reported that antigorite is a major component of serpentinite mylonite, which is cohesive and is characterized by a penetrative foliation and lineation (Norrell et al., 1989; Hermann et al., 2000; Li et al., 2004). Deformation experiments performed at pressures of 1–4 GPa and temperatures of 200–500 °C reveal that viscous relaxation times of antigorite have a range the equivalent of long-term deformations after large earthquakes to slow earthquakes at subduction zones (Hilairet et al., 2007). Based on frictional deformation studies performed at low temperatures and pressures, it has been proposed that antigorite is conducive to seismic slip at shallow crustal levels (Dengo and Logan, 1981; Moore et al., 1997; Reinen, 2000); however, at low temperatures it is chrysotile rather than antigorite that is stable, meaning that chrysotile is a potential agent of aseismic slip (Moore et al., 1997; Reinen, 2000).

Talc-bearing serpentinite is also thought to cause aseismic slip along the thrust boundaries of subducting plates, where the mantle wedge is serpentinized within the stability field of antigorite (Peacock and Hyndman, 1999; Hyndman and Peacock, 2003). Indeed, creep along the San Andreas Fault is attributed to the occurrence of talc-bearing serpentinite (Moore and Rymer, 2007; Wibberley, 2007). Several previous studies have undertaken petrological analyses of metasomatized serpentinites (e.g. Nishiyama, 1990; Schandl and Naldrett, 1992; Hansen et al., 2005; Spandler et al., 2008); however, the shear-deformation microstructures in such rocks have yet to be described in detail. Studies of natural examples of deformed serpentinite and associated metasomatic rocks are expected to provide new information on the rheology of subducting plate boundaries and major fault zones.

In this paper, we describe a meter–scale transition from serpentinite mylonite, which contains antigorite with a lattice

* Corresponding author. Tel.: +81 3 5286 9864; fax: +81 3 3207 4950.
E-mail address: soda@asagi.waseda.jp (Y. Soda).

0191-8141/$ – see front matter © 2010 Elsevier Ltd. All rights reserved.
doi:10.1016/j.jsg.2010.05.003

preferred orientation (LPO), to sheared metasomatic rocks (associated with brecciation) along the Sashu Fault, Japan, and go on to discuss the history of the shear deformation, P–T conditions, and the implications of our findings for the rheology of the fault zone.

2. Geological setting

The serpentinites examined in this study are exposed along the Sashu Fault upon the Saganoseki Peninsula, Southwest Japan (Fig. 1a). The Sashu Fault marks the boundary between the Sambagawa metamorphic rocks to the north and the structurally overlying Upper Cretaceous Onogawa Group to the south (Teraoka et al., 1992; Yamakita et al., 1995). At the western end of the fault, the Nishikawauchi Formation, a Jurassic accretionary complex, occurs as a small lenticular mass (Saito et al., 1993). The fault strikes approximately NE–SW and dips 20–70° to the SE.

The Sambagawa metamorphic rocks, which are distributed from Kanto to the Saganoseki Peninsula, underwent high-P/T metamorphism during the Cretaceous (Banno and Sakai, 1989; Wallis and Banno, 1990). On the Saganoseki Peninsula, Sambagawa metamorphic rocks consist mainly of pelitic and basic schists, with subsidiary psammitic and quartzose schists. The mineral assemblage within the pelitic schist is indicative of the

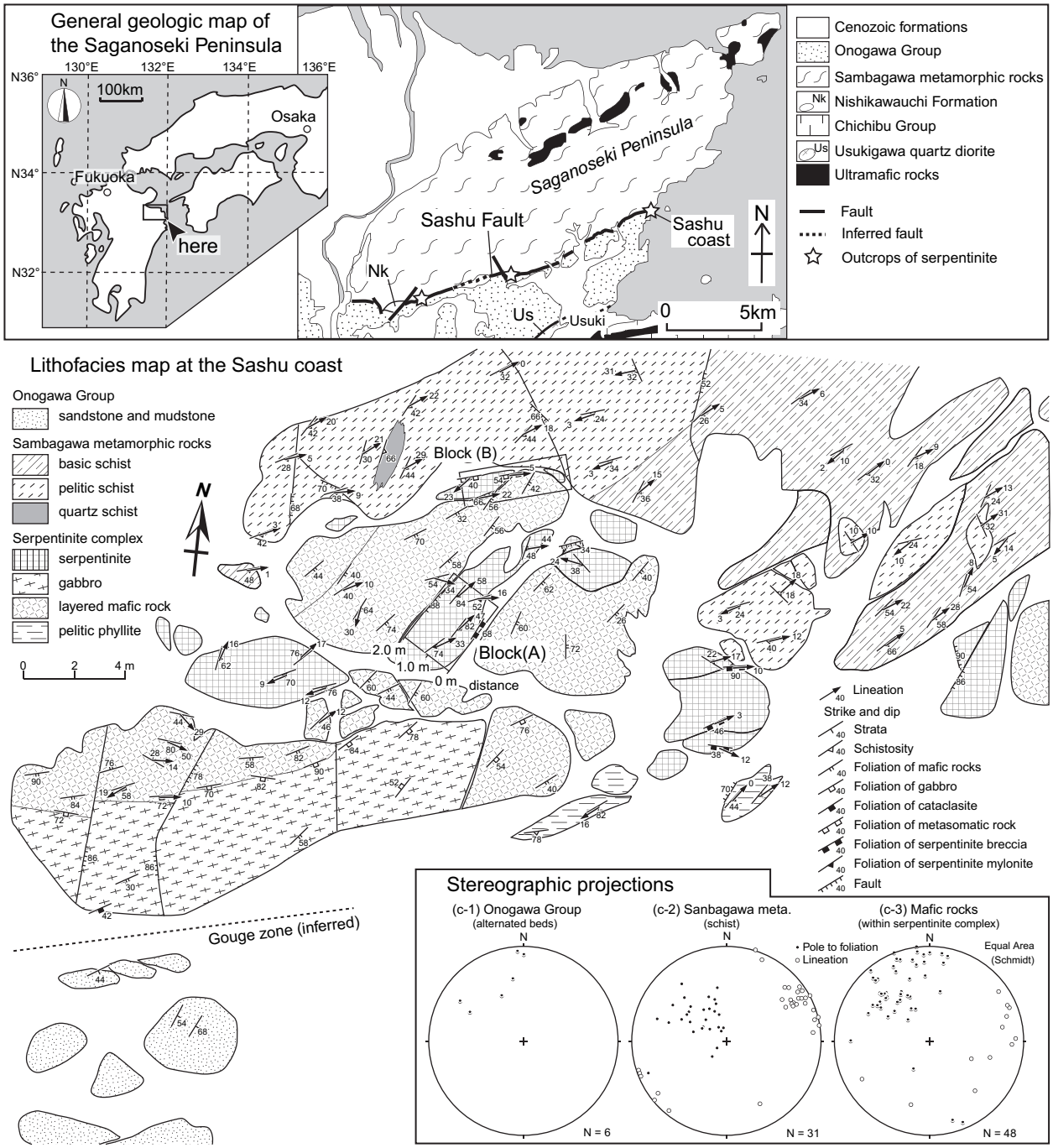

Fig. 1. (a) Geological map of the Saganoseki Peninsula, modified after Teraoka et al. (1992). (b) Lithofacies map of the outcrop on the Sashu coast. (c) Stereoplots showing structural data from outcrops along the Sashu coast (lower-hemisphere, equal-area projections).

upper part of the chlorite metamorphic zone (Miyazaki and Yoshioka, 1994), representing temperatures of 350–450 °C and pressures of 7–9 kbar (Banno and Sakai, 1989). The Onogawa Group consists of fore-arc basin sediments that define asymmetric synclinoria with axes plunging to the northeast (Teraoka, 1970). The uppermost formation within the Onogawa Group contains phyllite clasts that yield a K–Ar age of 190 Ma, correlating with the Suo metamorphic rocks (Isozaki and Itaya, 1989) rather than the Sambagawa metamorphic rocks (ca. 80 Ma).

The complex of serpentinites and mafic rocks is exposed discontinuously along the Sashu Fault. In the present study, we analyzed three outcrops of mylonitized serpentinite (Fig. 1a). Elsewhere along the fault, the Sambagawa metamorphic rocks are directly in contact with sedimentary rocks of the Onogawa Group, accompanied by fault gouge. The fault gouge records a top-to-the-west sense of shear (Yamakita et al., 1995).

3. Serpentinite complex on the Sashu coast

3.1. Terminology

The terms “serpentinite mylonite” (e.g. Norrell et al., 1989; Hermann et al., 2000; Li et al., 2004), “antigorite mylonite” (O’Hanley, 1996), and “antigorite schist” (Vogler, 1987) are applied to deformed but cohesive serpentinites with well-developed penetrative planar fabrics, and which consist almost entirely of antigorite. In this study, we use the term “serpentinite mylonite” as defined by Norrell et al. (1989) and emphasize that the serpentinites occur in a fault zone and contain non-foliated blocks. The terms “talc schist” and “chlorite schist” are used to describe foliated metasomatic rocks from the reaction zone along the fault (e.g. Nishiyama, 1990; Spandler et al., 2008). Note that the terms “mylonite” and “schist”, as used in this paper, are purely descriptive, without any implications regarding the type(s) of deformation mechanism(s) involved.

3.2. Occurrences of fault rock on the Sashu coast

The complex of serpentinite mylonite and mafic rocks along the Sashu Fault is well exposed along the Sashu coast, northeast of Usuki City (Fig. 1). Those rocks occur as blocks of less than 15 m in size within a complex that extends for 50 m along the fault. The serpentinite blocks make up about 30% of the complex. The complex is sandwiched between Sambagawa schists (to the north) and sedimentary rocks of the Onogawa Group (to the south). The Sambagawa metamorphic rocks are composed of pelitic and mafic schist, and even when immediately in contact with the serpentinite complex, they show little evidence of brittle deformation. The Onogawa Group consists of alternating beds of sandstone and mudstone that are boudinaged within 15 m of the fault. The central part of the southern margin of the complex contains phyllite blocks of 4 m in size. The Sashu Fault in this outcrop trends ENE–WSW, although the fault gouge zone is not exposed, being covered by gravel and sand.

Blocks of serpentinite mylonite are cohesive and hard, forming outcrops that resist erosion by wave action. Foliation and lineation within the serpentinite mylonite are barely discernible in outcrop because the serpentinite is fine-grained and homogeneous; consequently, these structures were measured in the laboratory from polished oriented samples (Fig. 2a). The foliation and lineation are defined by the alignment of opaque minerals and carbonate minerals set in an antigorite matrix. Foliation and lineation are developed throughout almost all the blocks, with the exception being one block at the southern end of the complex in which the foliation and lineation are developed heterogeneously. Brecciation overprints the serpentinite mylonite at the margin and tips of the block. The serpentinite mylonite and breccia blocks contain no exotic clasts.

The mafic rocks, another component of the complex, consist of layered mafic rocks and gabbro that are metamorphosed and partly mylonitized. The layered mafic rocks, which are green, schistose, and occasionally intercalated with white plagioclase-rich layers,

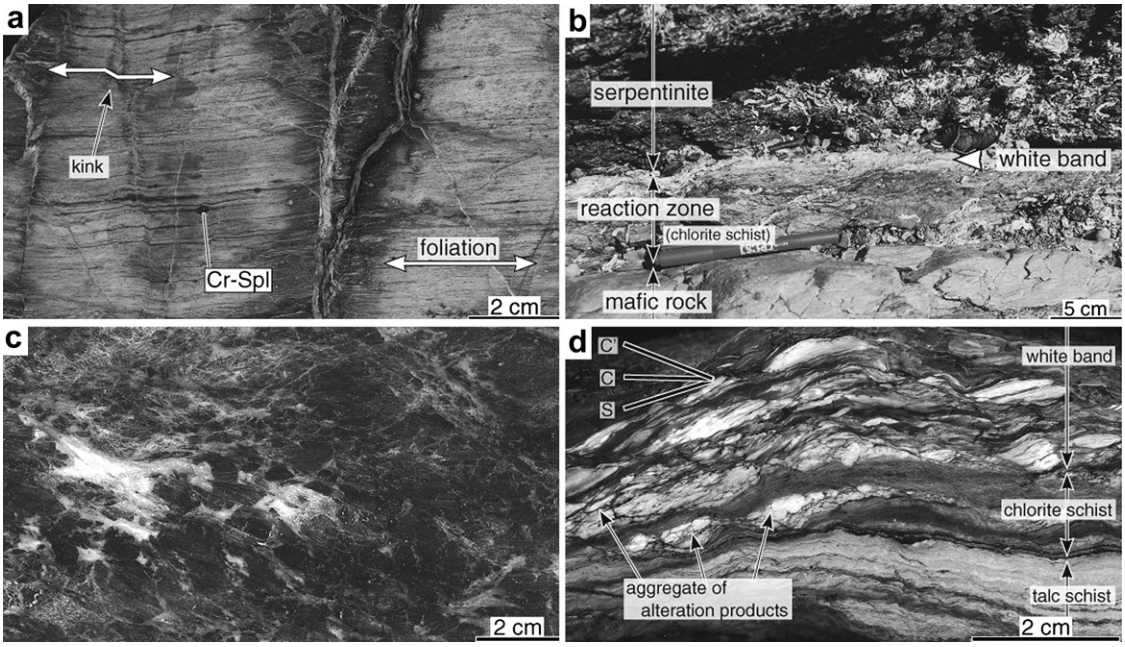

Fig. 2. Photographs of polished hand specimens (a, c, d) and an outcrop (b). (a) Serpentinite mylonite with a well-developed penetrative foliation. Kink bands (arrows) are partly developed. *XZ* section. Cr-Spl: Cr-spinel. (b) The reaction zone. Serpentinite in this zone is largely free of brecciation. (c) Calcite and talc infilling voids and fractures in the serpentinite breccia. (d) Sheared metasomatic rock of intercalated talc and chlorite schist, showing dextrally sheared composite planar fabrics. The S plane is defined by lenticular aggregates of alteration minerals (white color) that obliquely transect shear bands (C′). *XZ* section.

consist mainly of hornblende, plagioclase, epidote, and chlorite, with accessory titanite. The meta-gabbro consists mainly of varying proportions of coarse-grained hornblende and plagioclase.

Reaction zones, which are developed along the boundary between serpentinite and mafic rocks or pelitic schist of the country rock (Sambagawa metamorphic rocks) (Fig. 2b), consist of altered serpentinite breccia (Fig. 2c) and incohesive schistose metasomatic rocks such as talc and chlorite schist (Fig. 2d). Characteristic white bands (1–5 cm wide), made up of aggregates of fine-grained tremolite, chlorite and talc, are developed in reaction zone (Fig. 2b, d) where in contact with the highly chloritized mafic rocks and pelitic schist. From the margin to the centre of each block, the serpentinite shows a gradual change in structure from altered breccia to mylonite. Small serpentinite blocks are completely brecciated (e.g. block B in Fig. 1b), with the entire block constituting a reaction zone. The reaction zones are relatively soft, and tend to be eroded by wave action to form grooves between blocks. Fig. 3 summarizes the spatial relations between different rock types within the complex.

Foliation within the serpentinite complex strikes between ENE–WSW and NE–SW, dipping moderately to steeply to the south and southeast (Fig. 1c–3 4a). Lineation plunges to the ENE and WSW at 0–30°, with the ENE trend being dominant. The strike of schistosity within the Sambagawa metamorphic rocks is concordant with that in the serpentinite and mafic rocks, although the schist tends to dip southward at shallower angles than do the latter rocks (Fig. 1c-2). The orientation of strata within the Onogawa Group (Fig. 1c-1), where adjacent to the fault, is also concordant with the orientation of the fault zone. The metasomatic rocks strike approximately E–W (Fig. 4b), slightly oblique to the strike of other rock types. The traces of foliation in the mafic rocks are dragged toward the presumed fault gouge zone, indicating dextral movement along the fault (Fig. 1b).

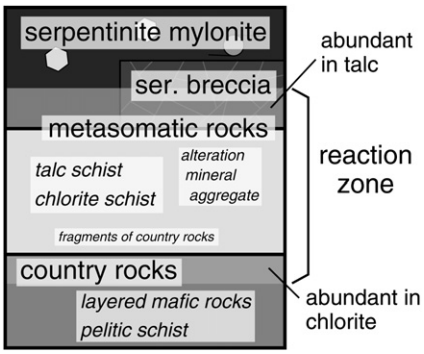

Fig. 3. Summary of the spatial relations among different rock types within the serpentinite complex.

4. Mineral assemblages and deformation structures of serpentinite and metasomatic rocks

4.1. Mineral assemblages within serpentinite

The constituent minerals of the serpentinites were identified using polarizing microscopy, electron probe microanalyzer (EPMA) analysis, X-ray diffraction, and cathodoluminescence microscopy. Laser Raman spectroscopy was used to identify serpentine polymorphs (Groppo et al., 2006). The foliated rocks were analyzed in thin sections cut parallel to the lineation and normal to the foliation (*XZ* plane), normal to the lineation (*YZ* plane), or parallel to the foliation (*XY* plane).

The serpentinites generally consist of antigorite with minor magnetite and Cr-spinel (Fig. 5a–e); carbonates and sulfides are also present in variable proportions. There are no primary peridotite minerals, but large blocky carbonates (>0.5 mm) (Fig. 5b) are probably pseudomorphs after peridotite minerals. These carbonates occasionally encompass platy and coarse-grained antigorite. Antigorite also occurs as platy or acicular crystals in the matrix and in veins. Cr-spinel is euhedral (ca. 2.0 mm in size) and contains small (<10 μm) inclusions of olivine, pyroxene, and pargasite. Fine-grained (<0.1 mm) magnetite is scattered throughout the serpentinite. The mineral assemblages within two representative blocks (Fig. 1b) are described specifically below (see also Table 1).

4.1.1. Mineral assemblages of serpentinite block (A)

Block (A) retains prominent serpentinite mylonite textures. At its centre, serpentinite mylonite is composed mainly of antigorite, magnetite, and carbonates, with accessory pyrrhotite and pentlandite (Table 1a). Carbonate minerals exist as blocky magnesite cut by veins of dolomite and calcite. Some dolomite overgrows the rims of blocky magnesite. Cathodoluminescence microscopy reveals multiple stages of carbonate precipitation in the veins.

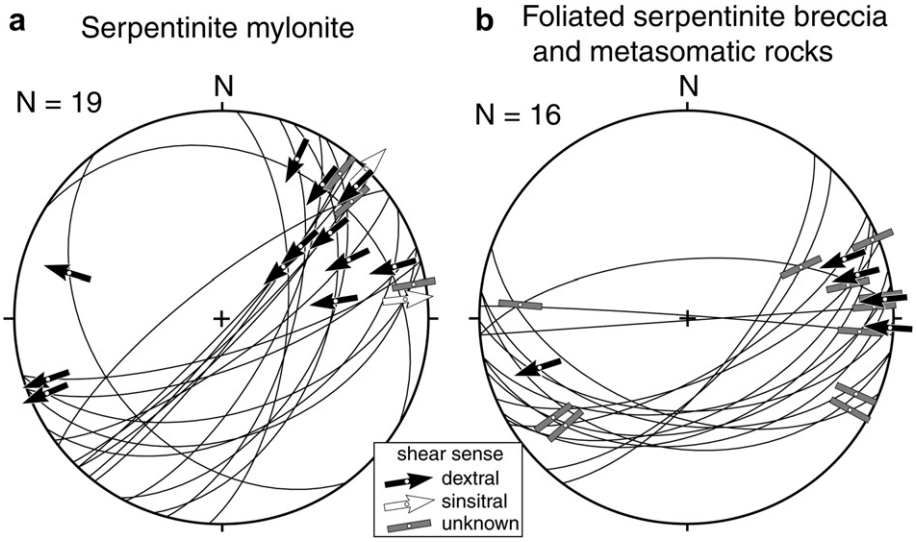

Fig. 4. Lower-hemisphere equal-area projections showing the orientations of foliation (great circles) and lineation (centre points of arrows and bars) within deformed serpentinites from the Sashu coast. (a) Serpentinite mylonite. (b) Foliated serpentinite breccia and foliated metasomatic rocks. Arrows indicate shear sense.

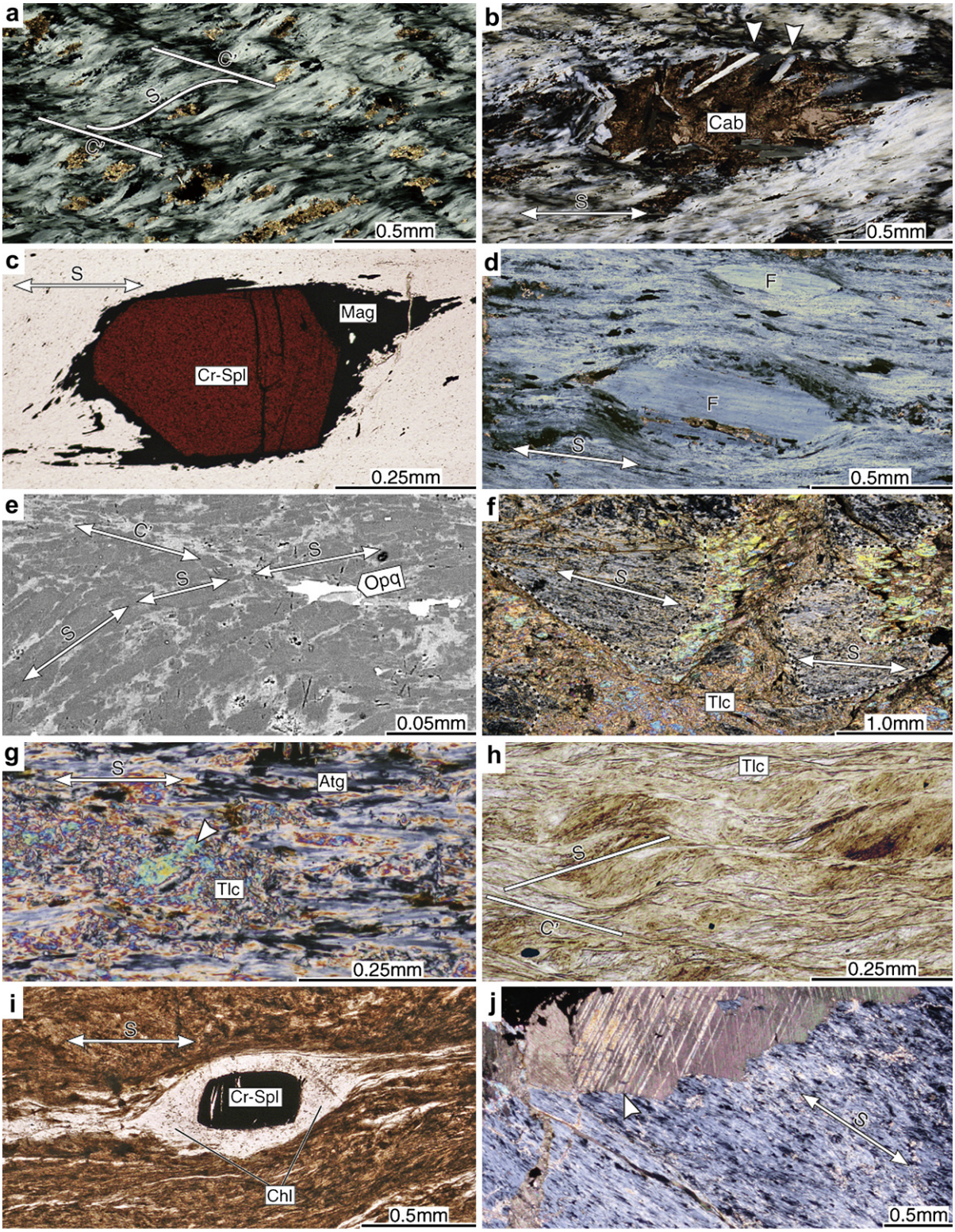

Fig. 5. Photomicrographs of serpentinites from the Sashu coast. (S) and (C′) indicate the S plane and C′ plane in each photomicrograph. (a) S–C′ fabric in serpentinite mylonite. Antigorite that defines an S plane is dragged toward the C′ plane. Crossed polarized light (CPL). (b) Blocky carbonate minerals (Cab). Coarse-grained platy antigorite (arrows) occurs in the carbonate. CPL. (c) σ-type Cr-spinel porphyroclast (Cr-Spl) with magnetite tails (Mag) showing dextral shear sense. Plane polarized light (PPL). (d) Antigorite "fish" (F) formed from an unusually large grain set among the S fabric antigorite. CPL. (e) Magnified BSE image of the S–C′ fabric. The S plane is dragged along the C′ plane. Light-gray area: Fe-rich antigorite; white area (Opq): opaque minerals. (f) Altered serpentinite breccia. Dashed lines indicate relics of serpentinite mylonite fragments suspend in a talc matrix (talc). CPL. (g) Moderately altered serpentinite. Antigorite (Atg) is replaced by Talc (Tlc), which shows post-kinematic growth (arrow). PPL. (h) Aggregate of altered minerals (light-brown) that define a composite planar fabric. Talc (Tlc) occurs in the colorless part of the image (relatively low refractive index). PPL. (i) Cr-spinel with a σ-type mantle of chlorite (Chl) within an aggregate of alteration minerals (brown area is matrix). PPL. (j) Serpentinite mylonite fragment and infilling of calcite in serpentinite breccia. The calcite contains type II deformation twins (arrow) (Burkhard, 1993). CPL.

Table 1
Mineral assemblages within blocks A and B (see the boxes in Fig. 1b). Distance in (a) indicates the sample location from the southeastern margin of block A.

(a) Mineral assemblages in the block (A)

Sample no.	Distance (m)	Antigorite	Magnesite	Dolomite	Calcite	Talc	Quartz	Magnetite Fe_3O_4	Pyrrhotite $Fe_{1-x}S$	Pyrite FeS	Cobaltite (Co,Fe)AsS	Pentlandite $(Fe,Ni)_9S_8$	Vaesite NiS_2	Bravoite $(Ni,Fe,Co)S_2$	Chalcopyrite $CuFeS_2$
A-1	2.0	○				○	○		○	○	○	○	○		
A-2	1.5	○	○	○	○		○	○	○	○	○	○			
A-3	1.1	○	○	○	○			○	○		○	○			
A-4	0.9	○	○	○	○			○	○			○			
A-5	0.9	○	○	○	○			○	○	○	○	○			
A-6	0.5	○		○	○			○	○			○			
A-7	0.3	○			○	○	○		○		○	○			○
A-8	0	○			○	○			○		○	○		○	○
A-9	0	○			○	○	○		○	○	○			○	

(b) Mineral assemblages in the block (B)

Sample no.	Rock name	Antigorite	Calcite	Talc	Pyrrhotite $Fe_{1-x}S$	Pyrite FeS	Cobaltite (Co,Fe)AsS	Pentlandite $(Fe,Ni)_9S_8$	Bravoite $(Ni,Fe,Co)S_2$	Chlorite	Tremolite/Actinolite	Sphene	Agrerate of alt. minerals
B-1	Ser. breccia	○		○		○	○	○					
B-2	Ser. breccia	○	○	○		○	○	○					
B-3	Talc schist	○		○	○	○			○				
B-4	Ser. breccia	○		○		○							
B-5	Chl. schist									○	○	○	○
B-6	Chl. schist		○							○	○	○	○
B-7	Talc schist	○	○	○				○					
B-8	Ser. mylonite	○	○	○	○	○		○					

Toward the margins of serpentinite blocks, the carbonate minerals change from magnesite and dolomite to solely calcite, which occurs as blocky, veins, and fine grains scattered throughout the antigorite matrix. Talc and sulfides replace antigorite and magnetite (Fig. 5g). Talc does not coexist with magnetite. Locally, quartz accompanies talc and carbonate minerals in veins. In the serpentinite breccia, fractures in the serpentinite are cemented by talc and calcite, where pyrite also occurs.

4.1.2. Mineral assemblages of serpentinite block (B)

Block (B) consists of altered serpentinite breccia, talc schist, and chlorite schist. The altered serpentinite breccia contains a higher proportion of metasomatic minerals than does the centre of block (A) (Table 1b). The growth of talc and calcite obscures the microstructural differences between fragments and veins in the breccia (Fig. 5f). The talc schist consists mainly of talc and minor Cr-spinel. The existence of Cr-spinel and occasional relics of antigorite with mylonitic microstructure indicates that the source rock of the talc schist was serpentinite mylonite and breccia.

Chlorite schist consists mainly of chlorite and aggregates of alteration products. Back-scattered electron (BSE) images and EPMA data show that the aggregates consist of various proportions of fine-grained tremolite, chlorite, and talc. The aggregates are brown to light-brown in color (Fig. 5h, i), display a weak cleavage, and are pleochroic. The source rocks of the chlorite schist are either serpentinite or the mafic rocks and pelitic schist. The former contain Cr-spinel (Fig. 5i), whereas the latter contain hornblende and titanite or quartz aggregates.

4.2. Deformation structures of serpentinites

4.2.1. Serpentinite mylonite

4.2.1.1. Microstructures in non-foliated serpentinite. In the non-foliated serpentinite, pseudomorphs after primary peridotite minerals are evident as blocky carbonates, outlined by fine-grained opaque minerals. Antigorite displays an interpenetrating texture characterized by platy and coarse-grained crystals ($\sim$0.5 mm long) or an interlocking texture composed of fine-grained acicular antigorite (O'Hanley, 1996). These microstructures show abrupt changes to mylonitic textures, even on the scale of a thin section.

4.2.1.2. Microstructures in serpentinite mylonite. Platy (or acicular) antigorite crystals are consistently about 0.05–0.3 mm long. Some coarse-grained antigorites (>0.5 mm) are similar in shape to mica-fish found in granitic mylonites (Fig. 5d). Platy antigorite displays a shape preferred orientation (SPO) that defines the foliation (S) and lineation, along with magnetite and carbonates. S and S–C′ fabrics are observed. The S fabric consists of an S plane defined by arrays of platy antigorite. Likewise, the S–C′ fabric (Fig. 5a) consists of S and C′ planes (shear bands) defined by arrays of platy antigorite. The distribution of C′ planes is inhomogeneous on the scale of a hand specimen. The angle between S and C′ planes is about 20–50°. The platy antigorite that defines the S planes is rotated toward the C′ planes (Fig. 5a). Outside of the blocky carbonate, coarse-grained platy antigorite grains that are contained in the carbonate are curved along the S or C′ planes in the matrix, or are truncated by new grains growing perpendicular to the old grains (Fig. 5b). Kink bands are locally developed within the S planes (Fig. 2a). Microfolds of S planes, with a half-wavelength of 3 mm, are observed locally in *YZ* thin sections, with fold axes oriented parallel to the mineral lineation and axial planes oriented parallel to the overall mylonitic foliation.

BSE images show that antigorite occurs as both platy-euhedral grains and euhedral Fe-rich grains. The modal abundance of Fe-rich antigorite is less than 10% and varies within individual blocks.

Along C′ planes, which include a small amount of Fe-rich antigorite, the margins of and fractures within platy-euhedral grains are cemented by Fe-rich anhedral antigorite (Fig. 5e). The grain size of these euhedral antigorites varies from 10 to 50 μm. The C′ planes are defined by antigorite and minor opaque minerals, and we observed no minerals that indicate the dehydration of antigorite (e.g. olivine or talc).

Antigorite veins contain carbonate minerals and talc, but not fine-grained magnetite. These veins occur as two textural types. The first is made up of plates that connect directly with platy antigorite grains that form S planes outside the vein. Such veins are locally linked to the formation of kink bands within S planes. The second type consists of fibrous antigorite with fibers oriented parallel to the vein wall, cross-cutting the antigorite fabrics outside the vein. Thus, these veins postdate the first type. Antigorite, especially in the second vein type, is pleochroic, varying from colorless to bright green.

Cr-spinel is accompanied by magnetite in mantle and tail structures that form σ-, δ-, and φ-type porphyroclasts (Fig. 5c). Shear sense indicators in the serpentinite mylonite indicate dextral movement (Fig. 4a).

4.2.1.3. Lattice preferred orientation of antigorite. To investigate whether the LPO of antigorite is a simple reflection of SPO in the serpentinite mylonite, we measured the optical directions of antigorite using a universal stage. The optic elastically axes of α, β, and γ in antigorite are approximately parallel to the crystallographic axes *c*, *a*, and *b*, respectively (strictly, only the *b*-axis is congruous with the optic elastically axis of γ) (Deer et al.,1992).

The antigorite fabric pattern for sample A (Fig. 6) was measured in an *XY* thin section cut parallel to the dominant S fabric. It is difficult to distinguish between the *a*-axis and *b*-axis in such a thin section, as the crystals in this orientation remain dark_under crossed polarized light when rotating the stage (the *c*-axis and the optic axis are sub-vertical). In this case, the *b*-axis can be identified once the optic axis has been found upon tilting the stage (the grain rapidly illuminates on the *b*-axis side of the optic axis). In the case that the optic axis is not clearly recognized, the *b*-axis is considered to be parallel to the long axis (and well-defined edge) of the grain. The fabric pattern shows that *b-axis* forms a point maximum parallel to the mylonite lineation; *c-axis* forms a *Z* point maximum normal to the mylonite foliation, with a minor girdle around the lineation; and *a-axis* forms a *Y* point maximum normal to the *XZ* section. In sample B, which has an S–C′ fabric, the occurrence of two peaks in the foliation (normal to *Z* and approximately 25° from *Z*) reflects the fact that *c-axis* of antigorite is normal to both the S and C′ planes (Fig. 6). This pattern is observed in an *XZ* thin section, and we measured 100 antigorite grains from both C′ and S planes. The obtained antigorite fabric patterns are similar to those reported by Vogler (1987) for samples from the Western Alps, as measured by X-ray texture goniometry.

4.2.2. Deformation and metasomatism of serpentinite after mylonitization

Serpentinite breccias show a jigsaw-puzzle texture (Fig. 2c) characterized by angular and irregularly shaped serpentinite fragments infiltrated by talc and calcite, occurring in the matrix or as veins. The size of serpentinite fragments varies from 1 to 20 mm. S–C′ and S fabrics are preserved in the serpentinite fragments (Fig. 5f, j). The proportion of fragments within the rock mass varies from 50 to 90%. Veins occasionally form an anastomosing network. The alignment of these serpentinite fragments defines a cataclastic foliation and lineation. Calcite in the matrix or veins of serpentinite breccia contains deformation twins (Fig. 5j) of type I, type II, and type III (Burkhard, 1993), with rare examples of Type III twins. Fluid inclusions are found in matrix calcite grains and veins within the serpentinite breccias.

Ghost textures of the mylonite are observed in moderately altered serpentinite. The antigorite that defines the mylonitic S and S–C′ fabrics is replaced by randomly oriented talc crystals (Fig. 5g). Although talc is abundant in these rocks, it shows replacement textures but not synkinematic growth textures.

4.3. Deformation structures in metasomatic rocks

Metasomatic rocks of variable mineral composition include talc schist, chlorite schist, and weakly altered fragments (or remnants) of country rock. These rocks contain asymmetric deformation microstructures that indicate dextral movement, as also observed in the serpentinite mylonites (Fig. 4b).

Drag folds are observed in the talc schist, with talc flakes (or needles) being curved within fold axes, showing undulose extinction. Chlorite schists, containing fragments of country rock, contain a composite planar fabric (Fig. 2d) in which S planes are defined by chlorite and the long axes of aggregates of altered minerals. Tremolite, talc, or calcite occasionally occur along C′ planes in the chlorite schist. Tremolite also overgrows porphyroclastic hornblende and fills fractures in hornblende within the chlorite schist. In the aggregates of altered minerals, fractures and extension cracks are cemented by chlorite and talc. The aggregates occasionally define the composite planar fabric, along with talc, along S and C′ planes (Fig. 5h). Cr-spinel in the aggregates is mantled by chlorite and is characterized by asymmetric clast-mantle shapes (Fig. 5i).

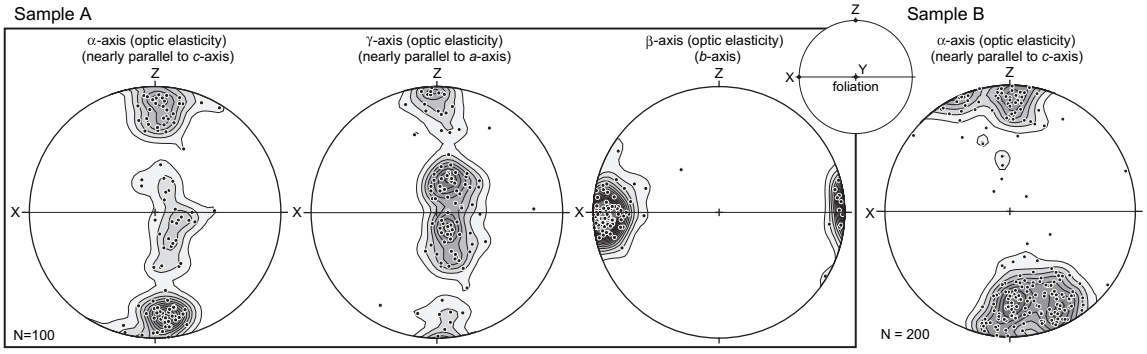

Fig. 6. Optical direction data for antigorite in serpentinite mylonite. Lower-hemisphere equal-area projections. *X* is the lineation in the serpentinite mylonite, and *Z* is the direction normal to the foliation. Contours represent the density of optical axial points by Gaussian counting. Sample A contains an S fabric, measured in an *XY* thin section. Sample B contains an S–C′ fabric, measured in an *XZ* thin section; 100 grains were measured for both S and C′ planes.

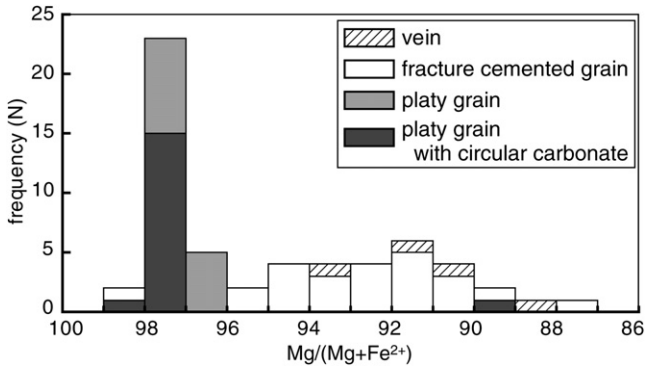

Fig. 7. Mg/(Mg + Fe^{2+}) values obtained for antigorite from serpentinite mylonites along the Sashu coast.

5. Mineral chemistry

The mineral chemistry of antigorite and chlorite was determined by wavelength-dispersive spectrometry (WDS) using a JEOL JXA-8900 at Waseda University, Japan, with the following settings: accelerating voltage, 15 kV; sample current, 1.2×10^{-8} A; and spot size, 10 or 2 μm.

5.1. Antigorite

The Mg mol fraction (Mg# = Mg/(Mg + Fe^{2+})) of the platy antigorite that defines S–C′ and S fabrics, and of the antigorite that accompanies the blocky carbonate minerals, varies within the narrow range 0.96–0.99 (Fig. 7). In contrast, the Mg# of grains that infill fractures and veins shows a wider range of 0.88–0.96. A small amount of Al is contained in the antigorite within the blocky carbonate (up to 0.4 wt%).

5.2. Chlorite

The analyzed chlorite consists of synkinematic grains in chlorite schist from a reaction zone adjacent to pelitic schist. The Al(IV) content in the tetrahedral site of chlorite varies from 6.0 to 6.4, corresponding to a temperature of 180–270 °C according to the geothermometer proposed by Cathelineau (1988).

6. Microthermometry of fluid inclusions within serpentinite breccia

6.1. Occurrence of fluid inclusions

The analyzed fluid inclusions occur in a single calcite vein (with minor talc) within the altered serpentinite breccia (Fig. 8a). The fluid inclusions are exceptionally large (5–10 μm in diameter). In other rocks, fluid inclusions are generally <5 μm in size, ruling out their use in microthermometric analyses. The present fluid inclusions are rhomboidal in shape, and consist of vapor and liquid phases. They are identified as primary fluid inclusions, based on the criteria proposed by Roedder (1984). Under cathode luminescence microscopy, the calcite shows no crack healing and the vein shows no evidence of multiple vein-forming events. The calcite contains type II deformation twins.

6.2. Analytical techniques and samples

Homogenization temperatures (Th) and the melting temperatures of ice (Tm) in the fluid inclusions were measured on a LINKAM TH600 fluid-inclusion stage. Incongruous values of Tm and Th (Fig. 8b, c) are explained by the small size of fluid inclusions, in which a vapor phase could not be recognized during Tm measurements. No double freezing (clathrate) was observed during the cooling experiments. The composition of liquid is within the H_2O–NaCl system, as indicated by a vapor phase moving slightly at the eutectic point during the heating of ice (up to −20 °C).

6.3. Results

Th ranges from 120 to 200 °C (mean = 155 ± 18 °C) and Tm ranges from −0.25 to −1.5 °C (Fig. 8). Salinity ranges from 0.4 to 2.6 wt% (NaCl equivalent), as calculated from Tm using the equation proposed by Bodnar (1993). Isochores of the fluid inclusions (Fig. 9) were determined following Bodnar and Vityk (1994).

7. Discussion

7.1. Chronology of serpentinite mylonitization, brecciation, metasomatism, and deformation

The geological events recorded in the fault rocks along the Sashu coast include serpentinite mylonitization, serpentinite brecciation, metasomatism, and deformation of the metasomatic rocks (Fig. 10). The chronology of these events is discussed below.

Although the deformation stage of serpentinite mylonitization is fundamentally distinct from the metasomatic stages, the observed microstructures of antigorite suggest that the final stages of serpentinite mylonitization were accompanied by weak metasomatism. Fe-rich antigorite, which occurs with metasomatic minerals in veins, crystallized after the early stages of formation of the mylonitic foliation (see Section 4.2). Previous studies have shown that antigorite is more stable at low temperatures when accompanied by carbonate minerals (O'Hanley, 1996). In addition,

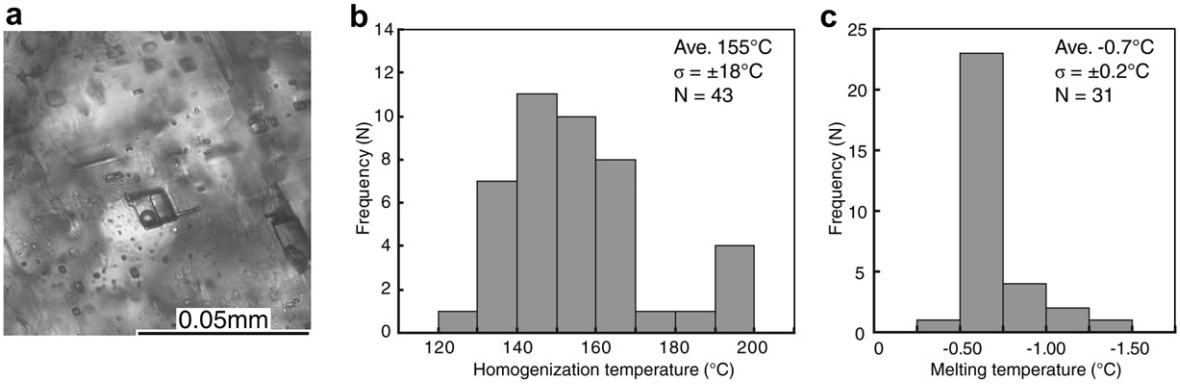

Fig. 8. Microthermometry of fluid inclusions from a calcite vein within serpentinite breccia. Photomicrograph of fluid inclusions (a), frequency histogram of homogenization temperatures (b), and melting temperatures (c) of fluid inclusions from a calcite vein within serpentinite breccia.

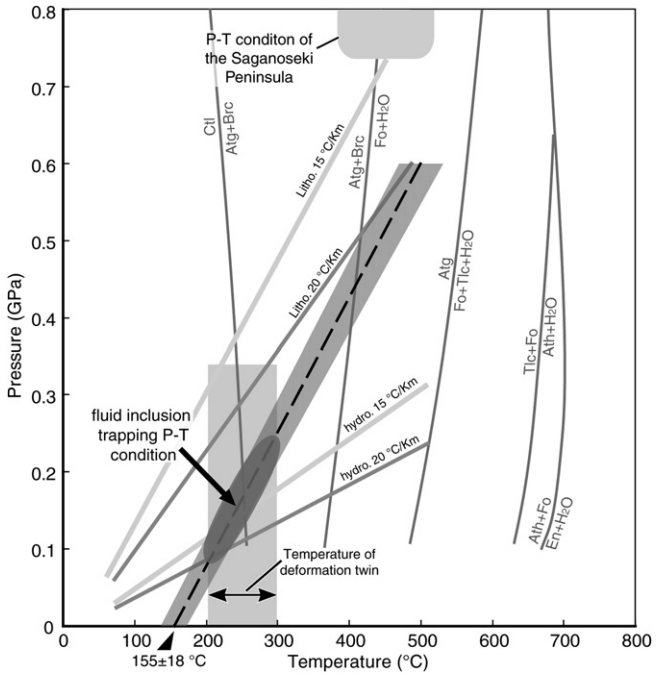

Fig. 9. Pressure–temperature diagram showing the estimated pressure of serpentinite brecciation. The salt-corrected (1.2 wt% NaCl equiv.) isochores represent the average homogenization temperature (dashed line) and one standard deviation (thin lines). Temperatures derived from the deformation twins are after Burkhard (1993). P–T conditions for a pelitic schist from the Saganoseki area were determined using the method proposed by Miyazaki and Yoshioka (1994). The fossil geothermal gradients are drawn with a range of 15–20 °C/km (Wallis and Banno, 1990) for hydrostatic and lithostatic conditions. Metamorphic reaction curves are after Bucher and Frey (2002). Atg: antigorite, Ath: anthophyllite, Brc: brucite, Ctl: chrysotile, En: enstatite, Fo: forsterite, Tlc: talc.

Fe-rich antigorite is considered to be stable under conditions of the lower blueschist facies and reducing conditions (Di Pierro et al., 2007), or under relatively low temperatures (<300 °C; Ribeiro Da Costa et al., 2008). These studies and our observations suggest that serpentinite mylonite deformation continued under weak metasomatic conditions.

Apart from Fe-rich antigorite, none of the metasomatic alteration minerals in the serpentinite mylonites show evidence of synkinematic growth. Carbonate minerals occur as pseudomorphs after primary peridotitic minerals, with no evidence of plastic deformation. The occurrences of carbonate minerals reveal that magnesite was the first carbonate phase to grow. Magnesite, as a replacement product of olivine, is commonly observed in metasomatized ultramafic rocks (e.g. Stanford, 1982; Hansen et al., 2005). The main stage of mylonitization had finished prior to metasomatism. Subsequent to mylonitization, brecciation of the serpentinite coincided with the formation and shearing of metasomatic rocks. The talc schist originated from serpentinite mylonite and breccia, but the metasomatic rocks are not themselves brecciated. These observations suggest that brecciation was synchronous with metasomatism, followed by ductile deformation of the metasomatic rocks.

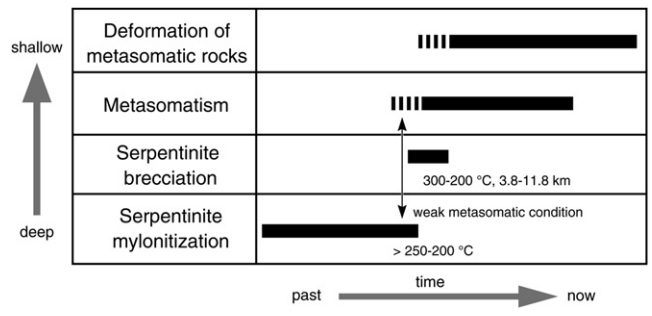

Fig. 10. Timing of serpentinite deformation events.

7.2. Deformation conditions during mylonitization of the serpentinite

Antigorite is stable within a relatively wide range of pressures and temperatures (O'Hanley, 1996; Ulmer and Trommsdorff, 1999). The upper temperature limit of antigorite stability is 600–700 °C at pressures of 1–4 GPa (Ulmer and Trommsdorff, 1999), and the lower limit is 200–250 °C at pressures of <2 GPa (O'Hanley, 1996). In addition, the lower limit of olivine stability is 350–450 °C (Ulmer and Trommsdorff, 1999). Previous studies have shown that pre-existing antigorite can undergo a partial dehydration near the upper limit of the antigorite stability field, and that olivine, clinohumite, and other dehydration minerals crystallize along C′ planes or within fractures during deformation (Scambelluri et al., 1991; Hermann et al., 2000).

Our observations indicate that the primary mineral assemblage of the serpentinite mylonite prior to metasomatism consisted of antigorite and primary olivine and pyroxene. The observed microstructures and LPO of antigorite show that the conditions of serpentinite mylonitization were within the stability field of antigorite. Considering the stability fields of antigorite and olivine, we suggest that the later stage of serpentinite mylonitization occurred below the temperature of the lower limit of olivine stability (350–450 °C). This interpretation is supported by the absence of dehydration minerals and their pseudomorphs along C′ planes in samples from the Sashu coast. However, it remains unclear whether this estimated temperature was maintained throughout the entire process of serpentinite mylonitization. Large plates of antigorite, accompanying olivine, are also found elsewhere in partially serpentinized peridotite (e.g. Mizukami and Wallis, 2005; Groppo et al., 2006) deformed under relatively high temperatures (<600–700 °C). Therefore, we suggest that the initial stages of serpentinite mylonitization occurred under relatively high temperatures, equivalent to the amphibolite facies, and that the final stages took place under greenschist or sub-greenschist facies conditions.

7.3. P-T conditions during serpentinite brecciation

Here, we estimate the temperatures and pressures during brecciation. Based on the isochore obtained in the microthermometric study (Fig. 9), a temperature (or pressure) correction is needed to determine the trapping temperature (or pressure) of the fluid inclusions. First, we discuss the temperature of brecciation.

Calcite deformation twins in the serpentinite breccia provide one measure of temperature in the breccias, although we must bear in mind that the twins formed after brecciation. Thus, the recorded calcite temperature provides a minimum value for the conditions of brecciation. Previous studies have documented the way in which different types of deformation twins reflect the temperatures during their formation (Burkhard, 1993; Ferrill et al., 2004). In the breccias described here, the type II and III deformation twins (which indicate temperatures of 200–300 °C; Burkhard, 1993) are the closest to recording the maximum temperature conditions of brecciation. The indicated temperature is supported by geothermometry using chlorite from schistose metasomatic rocks,

which gives a temperature of 180–270 °C. Accordingly, we propose that the serpentinite brecciation took place at temperatures of 200–300 °C. We can safely presume that the upper temperature limit of the brecciation was close to 300 °C because serpentinite mylonitization occurred at temperatures below 350 °C, as discussed above.

The isochore and temperature estimated from deformation twins corresponds to fluid pressures for the serpentinite breccia of 0.08–0.25 GPa (Fig. 9), possibly intermediate between hydrostatic and lithostatic pressures. Assuming the fluid inclusions were trapped under lithostatic conditions, the depth of brecciation would have been 3.0–9.4 km, based on a rock density of 2.7 g/cm^3. In contrast, assuming the fluid inclusions were trapped under hydrostatic conditions, the depth of brecciation would be deeper (8.1–25.5 km). However, the depth would have been less than 20 km, given the paleo-geothermal gradient of the Sambagawa metamorphic belt of approximately 15 °C/km (Wallis and Banno, 1990).

Considering fluid pressures that deviate from hydrostatic or lithostatic conditions, we now semi-quantitatively evaluate the fluid pressure during serpentinite brecciation. The pore fluid factor related to faulting, λ_v, has been discussed by many authors (e.g. Sibson, 1996, 2000; Streit and Cox, 2001; Clark and James, 2003). λ_v is defined as:

$$\lambda_v = P_f/\sigma_v = P_f/\rho g z$$

where P_f is fluid pressure, σ_v is vertical stress, ρ is the average rock density, g is gravitational acceleration, and z is depth. If P_f is hydrostatic, in the case of water-filled spaces connected with the surface, λ_v is approximately 0.4 (Sibson, 2003). It is estimated that P_f exceeds the hydrostatic conditions during fault activation. P_f is closer to the lithostatic condition in a compressional regime (λ_v: 1.0–0.8), and closer to hydrostatic conditions at shallow depths in extensional regimes (λ_v: 0.4–0.5). In the case of strike-slip faults, P_f takes an intermediate value (Sibson, 2000; Streit and Cox, 2001).

The present-day Sashu Fault dips to the southeast and shows strike-slip (dextral) movement. Yamakita et al. (1995) suggested that the Sashu Fault originally dipped moderately to the northwest, and that it was activated during the early Oligocene as a low-angle oblique thrust (top-to-the-west movement) for which the strike-slip component was twice the thrust component. Subsequently, the fault dipped to the southeast as part of an antiform with an NE–SW-trending fold axis. Given this scenario, P_f should not have a near-lithostatic value (λ_v; 0.8–1.0); consequently, the maximum value of λ_v is estimated to have been ~0.8. Accordingly, the depth of serpentinite brecciation is estimated to have been 3.8–11.8 km.

7.4. Role of metasomatic rocks in a subduction zone

A fundamental shift in the deformation of the studied serpentinite bodies occurred with a change in mineralogy from serpentinite to metasomatic rocks (e.g. talc and chlorite schist). In the case that serpentinite brecciation occurred at depths of 3.8–11.8 km, deformation of the metasomatic rocks would have continued at these depths or shallower. The depth of the Moho in continental subduction zones is estimated to be 20–50 km (e.g. Oleskevich et al., 1999; Bostock et al., 2002; Fujie et al., 2002). Therefore, the depths at which the studied serpentinites were deformed were shallower than the Moho, indicating that the serpentinite bodies were separated from the mantle and that the metasomatism and subsequent deformation may have occurred within crustal rocks or within sediments upon the subducting plate.

Fujie et al. (2002) and Mochizuki et al. (2005) reported aseismic slip within the Japan Trench off Sanriku, speculating that a thin layer with a low P-wave velocity exists along the plate boundary of the aseismic slip zone. The Moho in this region is below 20 km depth, and the thin layer exists at depths of 10–20 km. The authors suggested that the thin layer consists of clay minerals and serpentinite. It is reasonable to expect that this serpentinite layer was subjected to metasomatism in this setting, far from the Moho and where surrounded by crustal rocks. We suggest that these serpentinites are similar to the serpentinites of the present study.

Talc, being the softest of minerals, can reduce fault strength and induce stable sliding (Dengo and Logan, 1981; Peacock and Hyndman, 1999). Escartín et al. (2008) demonstrated that talc has a very low coefficient of internal friction and sliding friction, even at temperatures as high as 600 °C. Metasomatic talc may act as a lubricant and play a more important role in faulting than does serpentinite, regardless of the type of serpentine mineral. At subduction zones, metasomatic serpentinite bodies that ascend along the subduction interface may control the slip properties, even at depths shallower than the continental Moho.

8. Conclusions

This study describes the microstructures and deformation history of serpentinites from the Sashu Fault, Japan. The main conclusions of this study are as follows (Fig. 10).

The serpentinite mylonites are composed mainly of antigorite, display S or S–C′ fabrics, and contain porphyroclasts of Cr-spinel with tails of magnetite. Antigorite displays an LPO with a point maximum of *b* axes oriented parallel to the lineation. The serpentinite mylonitization occurred within the stability field of antigorite. Brittle deformation resulted in the formation of mylonitic serpentinite breccias, and the accompanying metasomatism occurred mainly in a reaction zone at the boundary between serpentinite and country rock. Talc and chlorite schist that developed in the reaction zone contain features of ductile deformation. The serpentinite brecciation occurred at temperatures of 200–300 °C and depths of 3.8–11.8 km, as estimated from fluid inclusions.

The serpentinites record a largely continuous deformation that involved mylonitization followed by brecciation (accompanied by metasomatism) and subsequent ongoing ductile deformation that affected some of the products of metasomatism. The mode of deformation of the serpentinite changes from an early, generally penetrative mylonitization during formation of the antigorite LPO to a later, more localized deformation during metasomatism in the reaction zone. The growth and occurrence of talc along the fault zone acted to weaken the fault, thereby promoting further deformation and enabling stable sliding.

Acknowledgements

We are grateful to Prof. M. Enjoji and Prof. Y. Ogasawara (Waseda Univ.) for their support in using the fluid-inclusion stage and the laser Raman spectroscope, respectively. Thanks are also due to Dr. I. Iwasaki and Dr. H. Arai (Waseda Univ.) for their comments and advice throughout this research, and to Mr. K. Yonemochi for assistance in using the EPMA. We thank the journal editor (Dr. Hippertt) and reviewers (Dr. Kanagawa and Dr. La Tour) for their constructive criticism and helpful suggestions. This work was supported by a Fukada Grant-in-Aid (2006) awarded to Y. Soda.

References

Andreani, M., Boullier, A.-M., Gratier, J.-P., 2005. Development of schistosity by dissolution-crystallization in a Californian serpentinite gouge. Journal of Structural Geology 27, 2256–2267.

Banno, S., Sakai, C., 1989. Geology and metamorphic evolution of the Sanbagawa metamorphic belt, Japan. In: Daly, J.S., Cliff, R.A., Yardley, B.W.D. (Eds.),

Evolution of Metamorphic Belts. Geological Society, London, Special Publication, no. 43, pp. 519–532.
Bodnar, R.J., 1993. Revised equation and table for determining the freezing point depression of H_2O–NaCl solutions. Geochimica et Cosmochimica Acta 57, 683–684.
Bodnar, R.J., Vityk, M.O., 1994. Interpretation of microthermometric data for H_2O–NaCl fluid inclusions. Short Course. In: De Vivo, B., Frezzotti, M.L. (Eds.), Fluid Inclusions in Minerals: Methods and Applications. IMA, pp. 117–130.
Bostock, M.G., Hyndman, R.D., Rondenay, S., Peacock, S.M., 2002. An inverted continental Moho and serpentinization of the forearc mantle. Nature 417, 536–538.
Bucher, K., Frey, M., 2002. Petrogenesis of Metamorphic Rocks, seventh ed. Springer, Berlin.
Burkhard, M., 1993. Calcite twins, their geometry, appearance and significance as stress–strain markers and indicators of tectonic regime: a review. Journal of Structural Geology 15, 351–368.
Cathelineau, M., 1988. Cation site occupancy in chlorites and illites as a function of temperature. Clay Minerals 23, 471–485.
Clark, C., James, P., 2003. Hydrothermal brecciation due to fluid pressure fluctuations: examples from the Olary Domain, South Australia. Tectonophysics 366, 187–206.
Deer, W.A., Howie, R.A., Zussman, J., 1992. An introduction to the rock-forming minerals, 2nd ed. Longman, England.
Dengo, C.A., Logan, J.M., 1981. Implications of the mechanical and frictional behavior of serpentinite to seismogenic faulting. Journal of Geophysical Research 86, 10771–10782.
Di Pierro, S., Compagnoni, R., Mellini, M., Groppo, C., Capitani, G., Belluso, E., 2007. Rock forming Fe-rich antigorite from low grade meta-ophicarbonates. Abstract Volume. In: Boullier, A.-M., Guillot, S., Quirico, E. (Eds.), Journées scientifiques "Serpentines". UJF, Grenoble, p. 16.
Escartín, J., Andreani, M., Hirth, G., Evans, B., 2008. Relationships between the microstructural evolution and the rheology of talc at elevated pressures and temperatures. Earth and Planetary Science Letters 268, 463–475.
Ferrill, D.A., Morris, A.P., Evans, M.A., Burkhard, M., Groshong Jr., R.H., Onasch, C.M., 2004. Calcite twin morphology: a low-temperature deformation geothermometer. Journal of Structural Geology 26, 1521–1529.
Fujie, G., Kasahara, J., Hino, R., Sato, T., Shinohara, M., Suyehiro, K., 2002. A significant relation between seismic activities and reflection intensities in the Japan Trench region. Geophysical Research Letters 29. doi:10.1029/2001GL 013764.
Groppo, C., Rinaudo, C., Cairo, S., Gastaldi, D., Compagnoni, R., 2006. Micro-Raman spectroscopy for a quick and reliable identification of serpentine minerals from ultramafics. European Journal of Mineralogy 18, 319–329.
Hansen, L.D., Dipple, G.M., Gordon, T.M., Kellett, D.A., 2005. Carbonated serpentinite (listwanite) at Atlin, British Columbia: a geological analogue to carbon dioxide sequestration. The Canadian Mineralogist 43, 225–239.
Hermann, J., Müntener, O., Scambelluri, M., 2000. The importance of serpentinite mylonites for subduction and exhumation of oceanic crust. Tectonophysics 327, 225–238.
Hilairet, N., Reynard, B., Wang, Y., Daniel, I., Merkel, S., Nishiyama, N., Petitgirard, S., 2007. High-pressure creep of serpentine, interseismic deformation, and initiation of subduction. Science 318, 1910–1913.
Hyndman, R.D., Peacock, S.M., 2003. Serpentinization of the forearc mantle. Earth and Planetary Science Letters 212, 417–432.
Isozaki, Y., Itaya, T., 1989. Origin of schist clasts of Upper Cretaceous Onogawa Group, Southwest Japan. Journal of the Geological Society of Japan 95, 361–368.
Li, X.-P., Rahn, M., Bucher, K., 2004. Serpentinites of the Zermatt–Saas ophiolite complex and their texture evolution. Journal of Metamorphic Geology 22, 159–177.
Miyazaki, K., Yoshioka, T., 1994. Geology of the Saganoseki district (with geological sheet map at 1:50,000). Geological Survey of Japan (in Japanese with English abstract).
Mizukami, T., Wallis, S.R., 2005. Structural and petrological constraints on the tectonic evolution of the garnet-lherzolite facies Higashi-akaishi peridotite body, Sanbagawa belt, SW Japan. Tectonics 24, TC6012. doi:10.1029/2004TC001733.
Mochizuki, K., Nakamura, M., Kasahara, J., Hino, R., Nishino, M., Kuwano, A., Nakamura, Y., Yamada, T., Shinohara, M., Sato, T., Moghaddam, P.P., Kanazawa, T., 2005. Intense *PP* reflection beneath the aseismic forearc slope of the Japan Trench subduction zone and its implication of aseismic slip subduction. Journal of Geophysical Research 110, B01302. doi:10.1029/2003JB002829.
Moore, D.E., Lockner, D.A., Ma, S., Summers, R., Byerlee, J.D., 1997. Strengths of serpentinite gouges at elevated temperatures. Journal of Geophysical Research 102 (B7), 14787–14801.
Moore, D.E., Rymer, M.J., 2007. Talc-bearing serpentinite and the creeping section of the San Andreas fault. Nature 448, 795–797.
Nishiyama, T., 1990. CO_2-metasomatism of a metabasite block in a serpentine melange from the Nishisonogi metamorphic rocks, southwest Japan. Contributions to Mineralogy and Petrology 104, 35–46.
Norrell, G.T., Teixell, A., Harper, G.D., 1989. Microstructure of serpentinite mylonites from the Josephine ophiolite and serpentinization in retrogressive shear zones, California. Geological Society of America Bulletin 101, 673–682.
O'Hanley, D.S., 1996. Serpentinites: records of tectonic and petrological history. In: Oxford Monographs on Geology and Geophysics, no. 34. Oxford University Press, New York.
Oleskevich, D.A., Hyndman, R.D., Wang, K., 1999. The updip and downdip limits to great subduction earthquakes: thermal and structural models of Cascadia, south Alaska, SW Japan, and Chile. Journal of Geophysical Research 104, 14965–14991.
Peacock, S.M., Hyndman, R.D., 1999. Hydrous minerals in the mantle wedge and the maximum depth of subduction thrust earthquakes. Geophysical Research Letters 26, 2517–2520.
Reinen, L.A., 2000. Seismic and aseismic slip indicators in serpentinite gouge. Geology 28, 135–138.
Ribeiro Da Costa, I., Barriga, F.J.A.S., Viti, C., Mellini, M., Wicks, F.J., 2008. Antigorite in deformed serpentinites from the Mid-Atlantic Ridge. European Journal of Mineralogy 20, 563–572.
Roedder, E., 1984. Fluid inclusions. In: Reviews in Mineralogy, vol. 12. Mineralogical Society of America.
Saito, M., Teraoka, Y., Miyazaki, K., Toshimitsu, S., 1993. Radiolarian fossils from the Nishikawauchi formation in the Onogawa Basin, east Kyushu, and their geological significance. Journal of the Geological Society of Japan 99, 479–482 (in Japanese).
Scambelluri, M., Hoogerduijn Strating, E.H., Piccardo, G.B., Vissers, R.L.M., Rampone, E., 1991. Alpine olivine- and titanian clinohumite-bearing assemblages in the Erro-Tobbio peridotite (Voltri Massif, NW Italy). Journal of Metamorphic Geology 9, 79–91.
Schandl, E.S., Naldrett, A.J., 1992. CO_2 metasomatism of serpentinites, south of Timmins, Ontario. Canadian Mineralogist 30, 93–108.
Sibson, R.H., 1996. Structural permeability of fluid-driven fault-fracture meshes. Journal of Structural Geology 18, 1031–1042.
Sibson, R.H., 2000. A brittle failure mode plot defining conditions for high-flux flow. Economic Geology 95, 41–48.
Sibson, R.H., 2003. Brittle-failure controls on maximum sustainable overpressure in different tectonic regimes. American Association of Petroleum Geologists Bulletin 87, 901–908.
Spandler, C., Hermann, J., Faure, K., Mavrogenes, J.A., Arculus, R.J., 2008. The importance of talc and chlorite "hybrid" rocks for volatile recycling through subduction zones; evidence from the high-pressure subduction mélange of New Caledonia. Contributions to Mineralogy and Petrology 155, 181–198.
Stanford, R.F., 1982. Growth of ultramafic reaction zones in greenschist to amphibolites facies metamorphism. American Journal of Science 282, 543–616.
Streit, J.E., Cox, S.F., 2001. Fluid pressures at hypocenters of moderate to large earthquakes. Journal of Geophysical Research 106 (B2), 2235–2243.
Teraoka, Y., 1970. Cretaceous formations in the Onogawa Basin and its vicinity, Kyushu, Southwest Japan. Report. Geological Survey of Japan 237 (in Japanese with English abstract).
Teraoka, Y., Miyazaki, K., Hoshizumi, H., Yoshioka, T., Sakai, A., Ono, K., 1992. Geology of the Inukai district (with geological sheet map at 1:50,000). Geological Survey of Japan (in Japanese with English abstract).
Ulmer, P., Trommsdorff, V., 1999. Phase relations of hydrous mantle subducting to 300 km. In: Fei, Y., Bertka, C.M., Mysen, B.O. (Eds.), Mantle Petrology: Field Observations and High Pressure Experimentation. Geochemical Society, Special Publication, no. 6, pp. 259–281. Huston, Texas.
Vogler, W.S., 1987. Fabric development in a fragment of Tethyan oceanic lithosphere from the Piemonte ophiolite nappe of the Western Alps, Valtournanche, Italy. Journal of Structural Geology 9, 935–953.
Wallis, S., Banno, S., 1990. The Sambagawa belt – trends in research. Journal of Metamorphic Geology 8, 393–399.
Wibberley, C., 2007. Talc at fault. Nature 448, 756–757.
Yamakita, S., Ito, T., Tanaka, H., Watanabe, H., 1995. Early Oligocene top-to-the-west motion along the Sashu fault, a low-angle oblique thrust of the Paleo-Median Tectonic Line, east Kyushu, Japan. Journal of the Geological Society of Japan 101, 978–988 (in Japanese with English abstract).